

# Quantification for contrast-enhanced digital breast tomosynthesis

Ann-Katherine Carton<sup>\*</sup>, Jingjing Li, Michael Albert, Sara Chen, Andrew D.A. Maidment  
Hospital of the University of Pennsylvania, 19104 Philadelphia, PA USA

## ABSTRACT

Digital breast tomosynthesis (DBT) is a tomographic technique in which individual slices through the breast are reconstructed from x-ray projection images acquired over a limited angular range. In contrast-enhanced DBT (CE-DBT) functional information can be observed by administration of an x-ray contrast agent. We have investigated the technical requirements necessary to quantitatively analyze CE-DBT exams. Using a simplified physiological model, a maximum aerial concentration of approximately 2.2 mg iodine/cm<sup>2</sup> in a 0.5 cm thick breast lesion is expected when administering 70 ml of 320 mg iodine/ml Visipaque-320®. This corresponds to a small change in x-ray transmission; up to 5 % for a 4 cm thick compressed breast. We have modeled CE-DBT acquisition by simulating Rh target x-ray spectra from 40 to 49 kV. Comparison of attenuation data of our simulated and measured spectra were found to agree well. We investigated the effect of scatter, patient motion and temporal stability of the detector on quantifying iodine uptake. These parameters were evaluated by means of experiments and theoretical modeling.

Keywords: Digital breast tomosynthesis, quantification, contrast agents, angiography

## 1. INTRODUCTION

Breast tumor growth and metastasis are accompanied by the development of new blood vessels<sup>1</sup>. These vessels are of poor quality and tend to leak. As a result, blood pools around the tumor. An imaging technique using a vascular contrast agent should be able to demonstrate and characterize the tumor and its vessels. Today, the best choice for imaging tumor vasculature in 3D is Contrast Enhanced-Magnetic Resonance imaging (CE-MRI) with a gadolinium based contrast agent<sup>2</sup>. CE-MRI is, however, expensive and time consuming and therefore unlikely to become widely available. We believe that Contrast-Enhanced Digital Breast Tomosynthesis (CE-DBT) would be a less expensive and less time consuming alternative to CE-MRI. It would potentially integrate the benefits of both CE digital mammography<sup>3-5</sup> and DBT<sup>6</sup>; thus, providing both functional information and improved breast cancer morphology by minimizing the superimposition of nonadjacent breast tissues that occurs with projection mammograms. Temporal analysis of contrast enhancement may further help to distinguish benign and malignant lesions.

In CE-DBT an iodinated contrast agent is used. The greatest subject contrast that can be produced with an iodinated contrast agent is by using x rays with energies just above the K-edge of iodine. In the experiments described, we have used temporal subtraction. High energy images are acquired before and after administration of the contrast agent<sup>3, 4</sup> (Figure 1). Logarithmic subtraction of these images is then performed. The signal intensities (SI) of the resulting images are proportional to the uptake of iodine.

The uptake of iodine in the breast is very small and thus causes only small changes in x-ray transmission; less than 5 %. This presents significant technical challenges if quantitative assessment of contrast agent uptake is desired. Technical factors that significantly influence quantitative analysis of CE-DBT exams are exposure reproducibility, linearity of the detector as a function of position, scatter, patient motion and temporal stability of the detector. In this paper, we will discuss scatter, patient motion and the temporal stability of the detector.

We have used a modified GE 2000D under IRB approval, to gain initial experience in CE-DBT. To date we have acquired 13 CE-DBT clinical cases.

---

<sup>\*</sup> [Ann-Katherine.Carton@uphs.upenn.edu](mailto:Ann-Katherine.Carton@uphs.upenn.edu); Phone: 215 746 8759; Fax: 215 746 8764

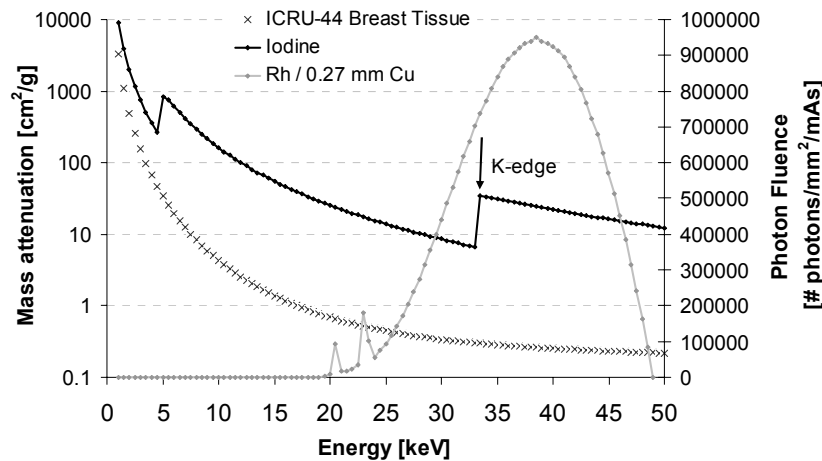


**Figure 1:** Mass attenuation data of ICRU-44 breast tissue and iodine. Example of a high energy x-ray spectrum from a Rh target exposed at 49 kV filtered with 0.27 mm Cu.

## 2. SIMPLE PHYSIOLOGICAL MODEL

We have developed a simple physiological model of breast tumors in order to determine the maximum uptake of a breast lesion. This uptake will be used as a point of comparison when considering factors which can alter the quantitative measurement of iodine uptake. We have considered a uniform contrast-agent/blood mixing model. Our model is based on the following assumptions: 1) the average adult has 5 l of blood pumped by the heart through the entire body in 1 min; 2) the time for an intravenous injection of contrast-agent is comparable to time for the heart to pump 5 l of blood; 3) the maximum concentration in the extracellular space is equal to the maximum intravascular concentration; and 4) the half-life of iodine in blood is long compared to the time of the clinical exam ( $\sim 10$  min). In our clinical trial, we used Visipaque-320® (320 mg iodine/ml iodixanol, Amersham, Princeton, NJ) injected at 1 ml/kg bodyweight followed by a saline flush. As an example, for a 70 ml Visipaque-320® injection, the maximum iodine concentration expected in the blood will be 4.5 mg/ml. In this instance, a 0.5 cm thick tumor would have an aerial density of  $\sim 2.2$  mg/cm<sup>2</sup>.

## 3. X-RAY SPECTRUM

We have modeled the x-ray spectrum in order to study how the quantification of iodine uptake is influenced by scatter, patient motion and temporal response of the detector. We simulated x-ray spectra in the range of 40 to 49 kV by extrapolating Boone's model<sup>7</sup>. Boone parameterized spectra measured at the FDA for Mo, Rh and W target x-ray tubes operated between 18 and 40 kV. Each energy bin in the spectra was fitted in terms of the photon fluence as a function of kV using first, second order or third order polynomials. We believe that these data are over-fitted. This will become evident when we consider how to extrapolate the data.

In this paper, we will only discuss the extrapolation of the Rh target spectra as Rh is the target that we have used to acquire our CE-DBT exams. The extrapolation was split in two parts. First, below 24 keV we used the parameters from Boone's paper for the extrapolated kVs. Second, above 24 keV, which we will refer to as the tails of the spectra, we refitted the spectra. In performing our fits, we assumed that: 1) for a given kV the photon fluence in the tails are linear with keV; 2) the slopes of the linear fits of the tails decrease with increasing kV; and 3) the photon fluence is zero at the maximum energy of each spectrum.

In Figure 2 we show spectra between 26 and 49 kV using Boone's parameters. Note that the shapes of the extrapolated spectra (grey) are similar to the published ones (black). Figure 2 b shows the low energy part in detail. The fluctuations in the extrapolated data are clearly artifactual. We have not addressed these artifacts as this low energy range is not of significance in imaging iodine. Next, consider the characteristic radiation peaks. Theoretically, for a thin target, the ratio of the  $K_{\alpha}$  to  $K_{\beta}$  peak is constant<sup>8</sup>; for a Rh target this ratio is 5.46. The target of an x-ray tube is not thin, but to a first approximation we can consider it as thin because the electrons incident on the anode are much less penetrating than the

fluorescent x rays. Figure 3 shows that  $K_{\alpha}/K_{\beta}$  decreases starting at 38 kV. This decrease may be due to erroneous fitting. However, it could also be explained by beam hardening in the thick Rh target. This would be consistent with our data, as beam hardening would cause the fraction of  $K_{\beta}$  to increase. Figure 2 c is a detail of the tails. Again one can see the effect of over-fitting. We could have kept the tails as they are and extrapolated them beyond 40 keV. However, as this energy range is of significance in imaging iodine, we chose to refit them. Using the assumptions stated above, we calculated the slopes of the tails for the spectra from 34 to 40 kV. The slopes were calculated from 26.5 keV using linear interpolation. We applied a least squares fit and used this fit to estimate the slopes of the tails of the extrapolated spectra. Figure 2 c shows our fits. In analogy with Boone's model, the photon fluences were fitted as function of kV for each energy bin. We applied first, second and third order fits. We chose the simplest fit for each energy bin. The residuals between the fits and the data were 2 orders of magnitude smaller than the actual data.

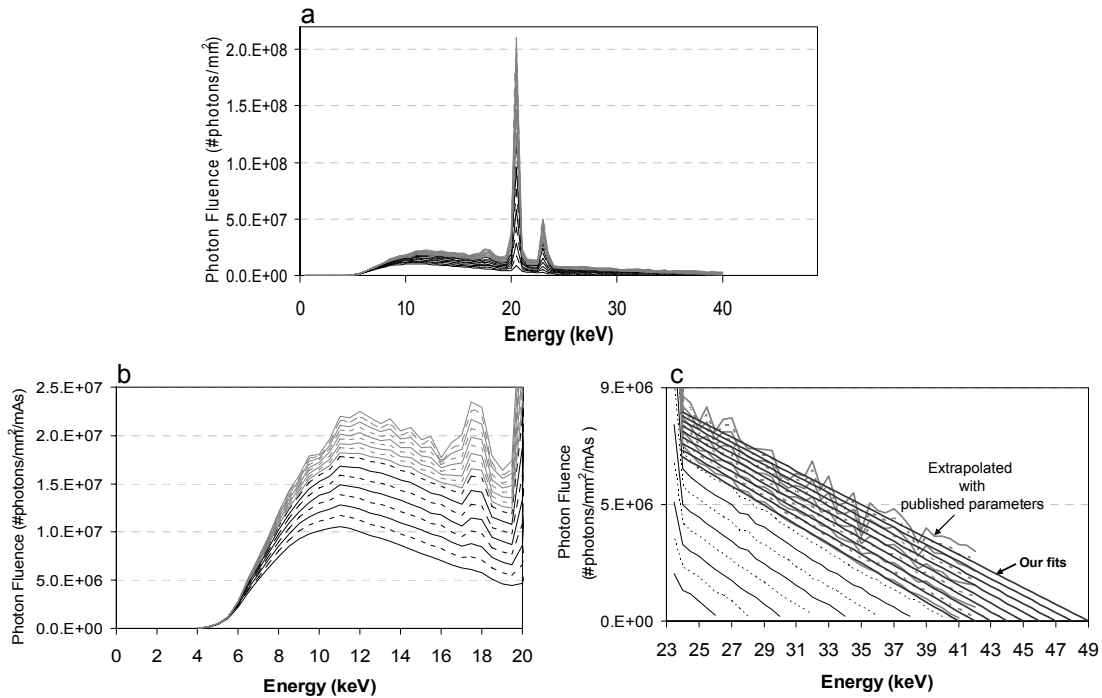
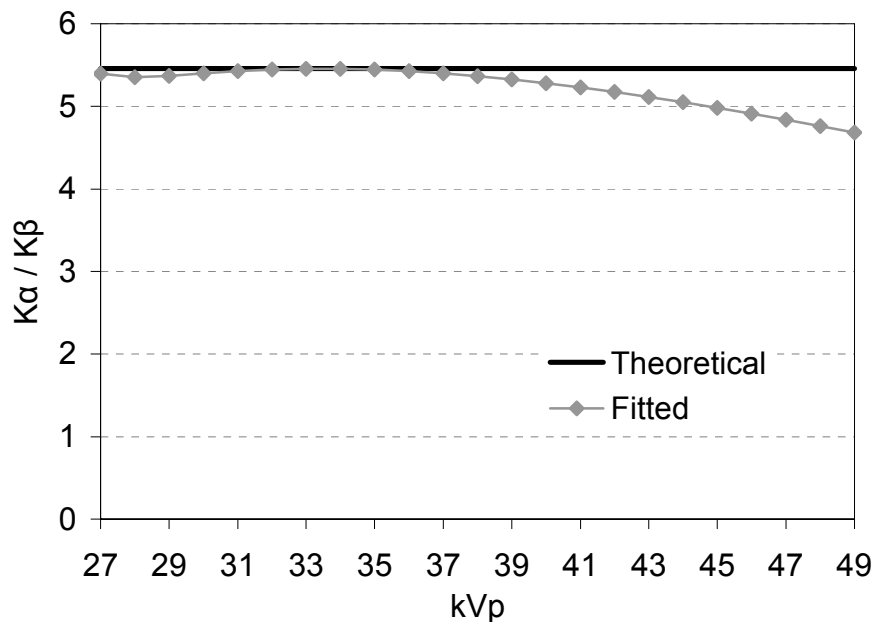


Figure 2: a) X-ray spectra from 26 kV to 49 kV using Boone's parameters. Note that the extrapolated spectra (grey) have the same shape as the published spectra by Boone (black). b) Detail of the low-energy region of the spectra shown in a). Note that the fluctuations in the extrapolated spectra are artifactual. c) Detail of the tails of the spectra shown in a). These fluctuations are also artifactual.

We validated our simulations using a least-squares comparison (i.e., minimizing the  $\chi^2$  values) between measured and simulated attenuation data. We used Al filters (99.997 % pure, Alfa Aesar, Ward Hill, MA) to determine the attenuation curves. The minimum  $\chi^2$  was found by adjusting the kV ( $kV_{\text{equivalent}}$ ) and adding extra Al ( $Al_{\text{equivalent}}$ ) to the simulated spectra. We also compared the half value layers (HVL), quarter value layers (QVL), eight value layers (EVL) and tenth value layers (TVL) of the measurements and the simulations. The measurements were performed with a Senographe 2000D (GE Medical Systems, Milwaukee, WI). The Senographe 2000D was operated with a Rh target and 0.25 mm Rh or 0.27 mm Cu filtration. We used the Cu filter to emphasize the tails. The tube has a 0.69 mm thick Be window; a 2 mm thick compression paddle was in the x-ray beam; the distance from the target to the exposure meter was 43 cm.

We modeled this system by filtering our fitted Rh spectra with added filtration simulated to match the experimental setup. Tables 1 and 2 demonstrate that the extrapolation of Boone's spectral models agree well with our measurements. Shown are the equivalent kV ( $kV_{\text{equivalent}}$ ) and equivalent Al filtration ( $Al_{\text{equivalent}}$ ) of the simulated spectra for a nominal kV that results in the smallest  $\chi^2$ . HVL and QVL are also presented for Rh and Cu filters; EVL and TVL are only presented for the Rh filter. The largest difference between the measured and simulated HVL, QVL, EVL and TVL is 1.8 % for the QVL at 49 kV with a Rh filter (48  $kV_{\text{equivalent}}$  and 0 mm  $Al_{\text{equivalent}}$ ). Figure 5 show examples of Rh spectra

filtered with 0.27 mm Cu. The largest difference between the measured and simulated HVL and QVL is 1.3 % for the QVL at 34 kV (33.5 kV<sub>equivalent</sub> and 0 mm Al<sub>equivalent</sub>). This occurs in the range of energies fitted by Boone. In the extrapolated range, the largest difference, 0.6 %, was found for the QVL at 49 kV (48.4 kV<sub>equivalent</sub> and 0 mm Al<sub>equivalent</sub>).



**Figure 3:**  $K_{\alpha}/K_{\beta}$  for a thin Rh target (theoretical) and as calculated in the fitted spectra. Note that  $K_{\alpha}/K_{\beta}$  decreases from 38 kV.

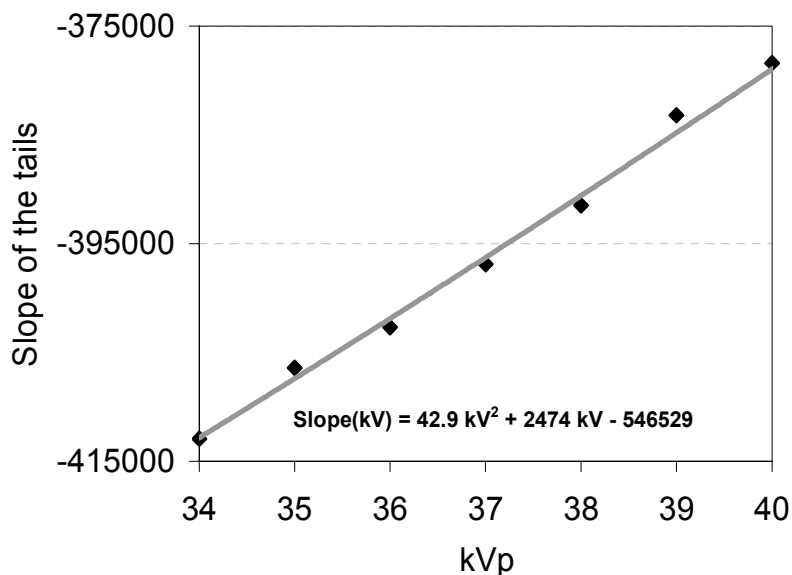


**Figure 4:** Slopes of the tails for the published spectra from 34 to 40 kV. A least squares fit was used to determine the slopes of the tails of the extrapolated spectra.

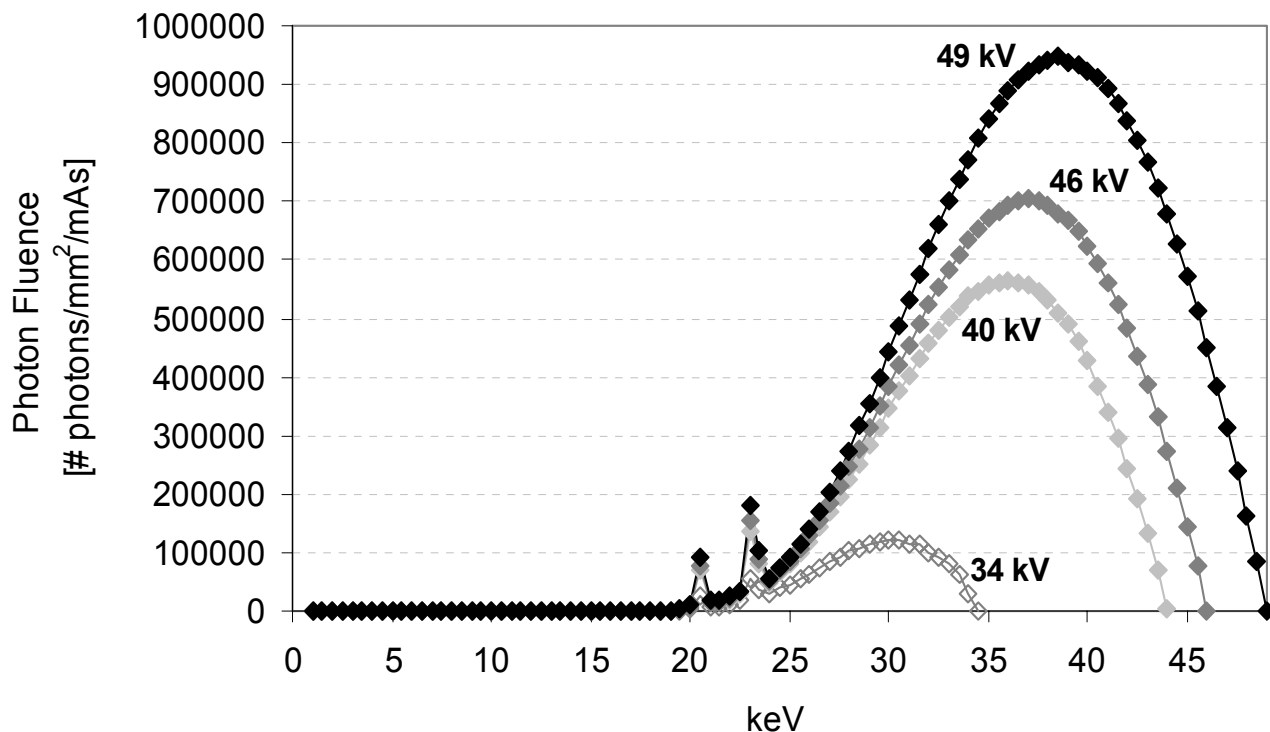


**Figure 5:** Examples of x-ray spectra from a Rh target filtered with 0.27 mm Cu. The fluence is specified 43 cm from the target.

**Table 1:** Comparison of the measured and simulated attenuation data for a Rh target filtered with 0.25 mm Rh. HVL, QVL, EVL and TVL are expressed in mm Al.

Nominal kV	kV <sub>equivalent</sub>	Al <sub>equivalent</sub>	Measured				Simulated				
			HVL	QVL	EVL	TVL	HVL	QVL	EVL	TVL	X <sup>2</sup>
25	25.3	0.000	0.361	0.820	1.382	1.574	0.359	0.822	1.378	1.573	0.0001
28	28.4	0.000	0.412	0.949	1.589	1.818	0.411	0.950	1.593	1.819	0.0001
34	33.5	0.000	0.478	1.116	1.868	2.120	0.482	1.114	1.859	2.118	0.0001
40	39.8	0.000	0.556	1.244	2.088	2.382	0.546	1.258	2.092	2.384	0.0001
46	45.0	0.000	0.578	1.341	2.228	2.575	0.586	1.346	2.243	2.563	0.0005
49	48.0	0.000	0.612	1.365	2.309	2.625	0.605	1.390	2.325	2.662	0.0006

**Table 2:** Comparison of the measured and simulated attenuation data for a Rh target filtered with 0.27 mm Cu. HVL and QVL are expressed in mm Al.

Nominal kV	kV <sub>equivalent</sub>	Al <sub>equivalent</sub>	Measured		Simulated		
			HVL	QVL	HVL	QVL	X <sup>2</sup>
34	33.5	0.0	1.711	3.532	1.713	3.579	0.0001
40	39.4	0.0	2.232	4.750	2.238	4.738	0.0001
46	45.5	0.0	2.779	5.978	2.787	5.978	0.0001
49	48.4	0.0	3.060	6.619	3.063	6.578	0.0001

## 4. SCATTER

We performed CE-DBT without a grid. We have performed experiments to determine the effect of scatter on the quantification of iodine uptake. The magnitude of the scatter was determined using the scatter fraction,  $SF$ :

$$SF = \frac{S}{S + P}$$

where  $S$  is scatter and  $P$  is primary radiation.  $SF$  was measured with Pb-disks<sup>9</sup> with diameters from 3.9 to 11 mm. The signal intensities (SI) in the shadows of the Pb-disks and in an unperturbed ROI were measured. The logarithms of the measured  $SF$  as a function of Pb-disk diameter were plotted. The inverse logarithm at zero disk diameter of a linear fit through the measured values gave the  $SF$  for an infinitesimally small disk. These measurements were repeated as a function of position and breast equivalent thickness in 50 % glandular-50 % fatty breast equivalent phantoms (CIRS, Norfolk, VA). The phantoms were positioned so as to mimic the MLO position, including higher order scatter from the chest (Figure 6 a). A 49 kV spectrum with a 0.27 mm Cu filter was used.

### 4.1. Scatter dependence as a function of position in the breast.

Figure 6 b shows the  $SF$  as a function of position in the breast. The  $SF$  is smaller at the lateral sides of the breast equivalent phantoms. The  $SF$  is slightly asymmetric across the centerline of the breast phantom. As expected, the  $SF$  increases from the chest wall side towards the center of the breast and then falls off again towards the nipple side. The  $SF$  varies significantly over the field of view. For example, for a 60 mm 50 % glandular-50 % fatty breast equivalent phantom, the  $SF$  at the edge of the breast phantom is 0.31, but it increases to 0.52 near the center of the field.

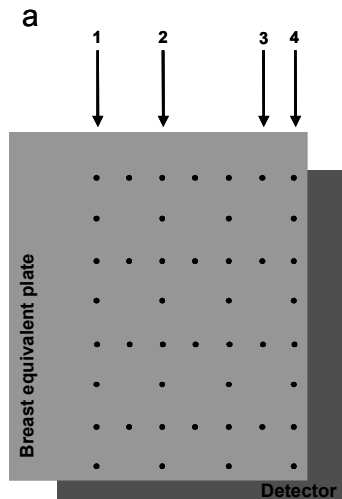
### 4.2. Scatter dependence as a function of breast thickness.

Figure 6 c illustrates  $SF$  profiles for 2 cm, 4 cm, 6 cm and 8 cm thick breast equivalent phantoms. The  $SF$  profiles are shown for the position in the phantom labeled "2" in Figure 6 a. As expected, the  $SF$  is higher for thicker breasts.

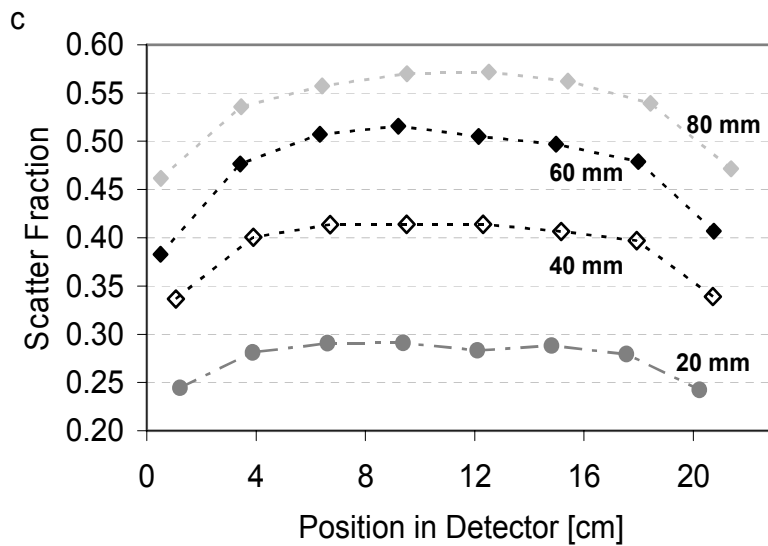
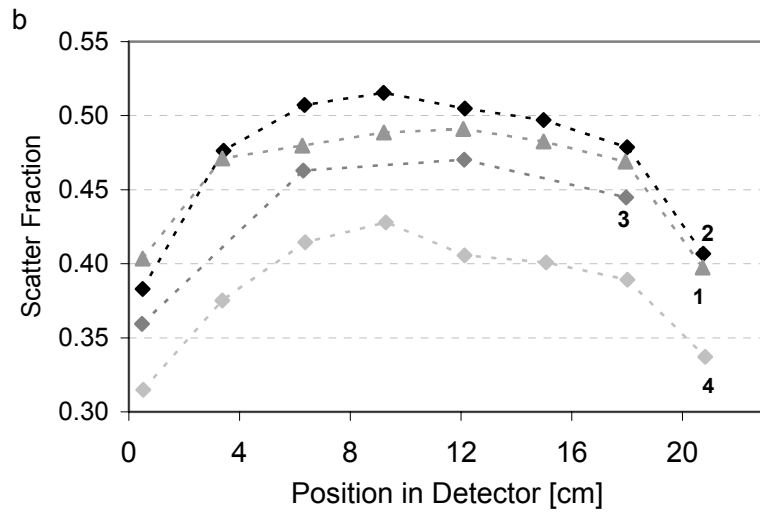
### 4.3. Effect of scatter on the quantification of the iodine concentration

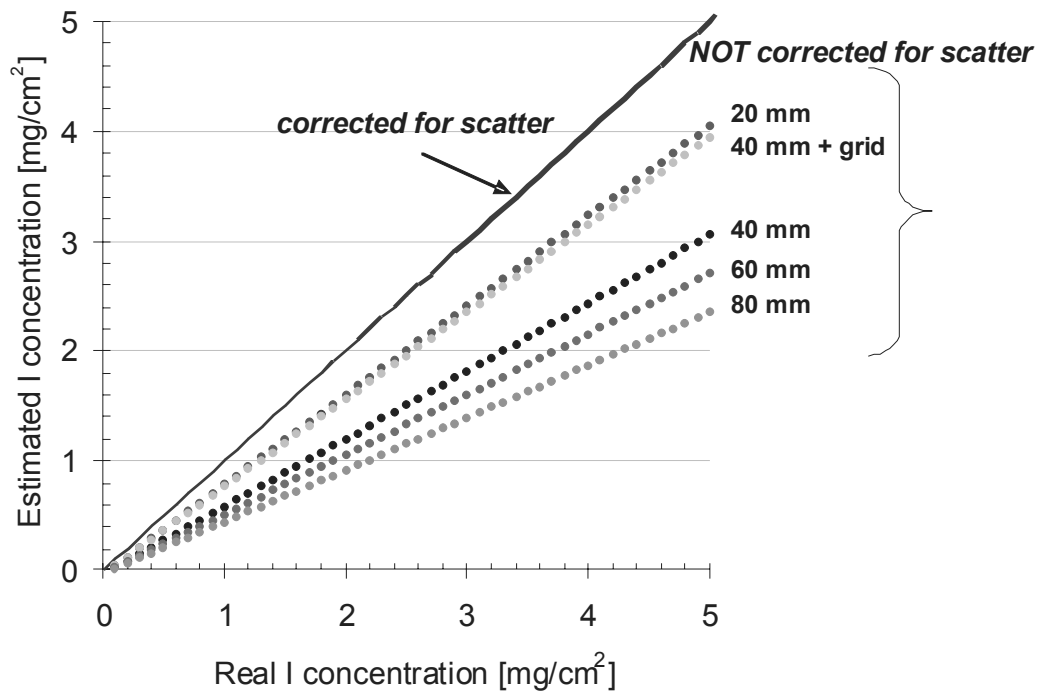
We modeled the effect of scatter on the quantification of the iodine concentration for various breast thicknesses. To do so, we simulated a Senographe 2000D tube operated at 49 kV with a Rh target and 0.27 mm Cu filtration. The simulation includes the attenuation of the Be-window, Cu-filter, compression plate, air, ICRU-44 breast tissue, and the CsI detector. We used the  $SF$  measured near the center of the breast equivalent phantoms. We calculated the contrast as a function of iodine uptake for the various breast thicknesses and calculated then the error in the iodine concentration estimate due to the scatter.

Figure 7 shows the extent to which the iodine concentration will be underestimated if not corrected for scatter. For example, consider a 2.5 mg/cm<sup>2</sup> iodine concentration. Failure to correct for scatter will result in an underestimation of the iodine concentration by 28 % for a 20 mm breast thickness, 40 % for a 40 mm breast thickness, 47 % for a 60 mm breast thickness and 54 % for a 80 mm breast thickness. Failure to correct for scatter when using a grid also results in an underestimation of the iodine concentration by 22 % for a 40 mm thick breast. This is relevant for quantitative CE-digital mammography.



**Figure 6:** Experimental set-up for the scatter measurements. The arrows indicate the positions along which  $SF$  are plotted in b) and c). b)  $SF$  as a function of position in a 60 mm thick breast equivalent phantom. c)  $SF$  as a function of breast thickness for the position indicated by arrow 2 in a).





**Figure 7:** Iodine concentration will be underestimated if not corrected for scatter. The simulation parameters were a Rh target, 49 kV and 0.27 mm Cu filter. No grid was used except where specified.

## 5. PATIENT MOTION

In temporal subtraction, images from pre-and post-contrast series are subtracted. Any breast motion between series will result in artifacts. In our experiments with patients, the total acquisition time can exceed 10 minutes. Breast motion is inevitable. We calculated the following measure to demonstrate the effect of breast motion on the estimated iodine uptake. In patient images, we selected ROIs with uniform breast thickness. The absolute values of relative SI variations were calculated between pixel positions that are  $\Delta x$  apart from each other. We varied  $\Delta x$  from 1 to 128 pixels (0.1 - 12.8 mm). We used  $SF$  measured near the center of the breast equivalent phantoms.

We calculated the contrast as a function of iodine uptake for the various displacements and then calculated the error in the iodine concentration estimate due to the displacements. These measurements were calculated for displacements in the horizontal and vertical direction. The relative SI variations were related to the corresponding estimates of iodine concentration to demonstrate the effect of motion on the quantification of iodine. Figure 8 a shows the SI in a homogenous ROI of a breast image acquired at 49 kV with a 0.27 mm Cu filter. The  $SF$  in this 45 mm thick ROI was  $\sim 0.40$ . Figure 8 b and c show the relative SI variations arising from various displacements. Even for 1 pixel (0.1 mm) displacements, half of the pixel signal intensities vary by 0.7 % and the maximum change is 4.7 % (Figure 8 d). A 4.7 % SI variation would correspond to 2.3 mg/cm<sup>2</sup> iodine. That is greater than the 2.2 mg/cm<sup>2</sup> iodine that we predicted with our simple physiological model for a 0.5 cm lesion.

A clinical example of patient motion is illustrated in Figure 9. The image is the difference of a post-contrast projection image and a pre-contrast projection image. Two lead BBs were placed near the nipple of the patient. The arrows in the image demonstrate examples of patient motion. The lower BB shows a displacement of approximately 5 mm. We have found that the greatest motion in the breast generally occurs in the dependent (lower) portion of the breast.

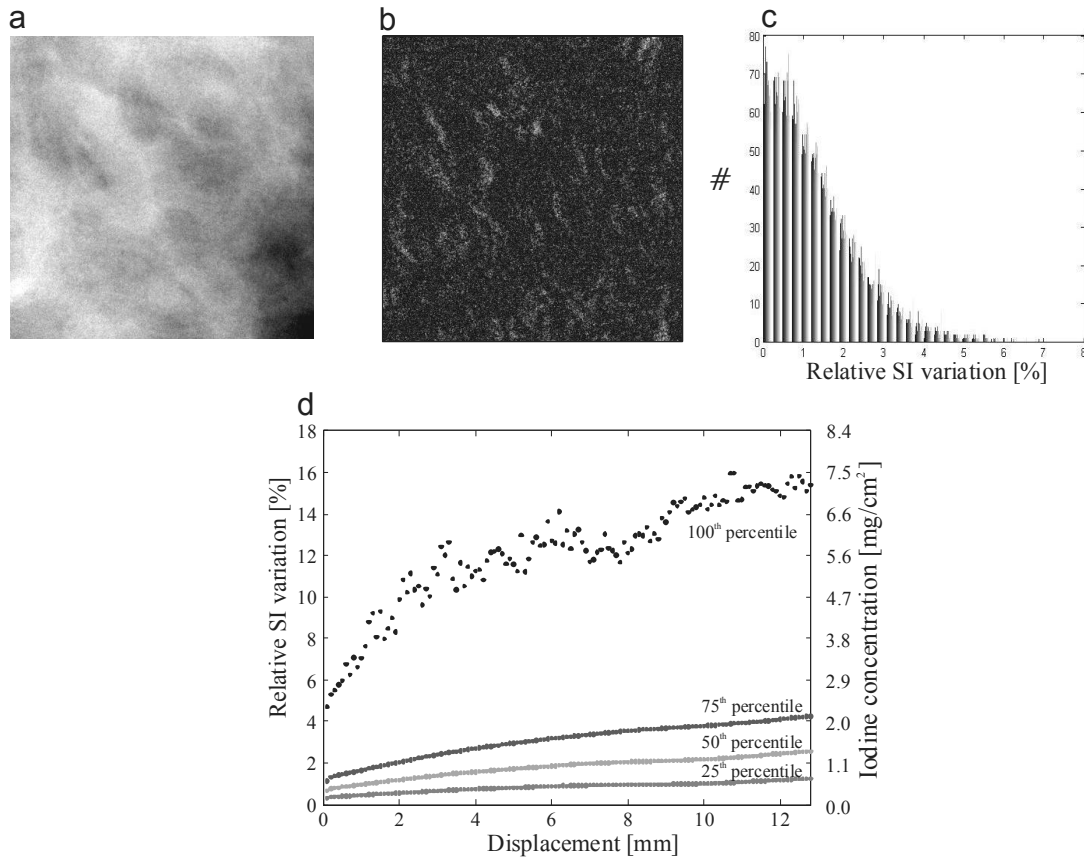


**Figure 8:** a) Example of a homogeneous ROI in a pre-contrast mammogram that has been acquired with a Rh target at 49 kV and with 0.27 mm Cu. b) Relative SI variations obtained by subtracting the ROI in a) shifted by 1 mm in the horizontal direction. c) Histogram of the relative SI variations shown in b). d) Relative SI variations arising from various displacements. The relative SI variations are equated with iodine uptake.

## 6. DETECTOR: TEMPORAL STABILITY

The stability of the temporal response of the detector depends on the exposure level, time delay between acquisitions and breast thickness<sup>10</sup>. Our experiments confirm the results presented by Jeunehomme *et al*<sup>10</sup>. The timing of the clinical CE-DBT projection images in our clinical trial at the University of Pennsylvania is as follows: nine projections are acquired while sweeping the x-ray tube over a 50° arc; one projection is acquired every 30 s; the first post-contrast image is obtained 90 s after the start of the contrast injection, and the x-ray tube is again swept over a 50° arc.

Figure 10 illustrates the relative SI variation as a function of time for a typical clinical acquisition sequence. A 40 mm PMMA plate was exposed at 49 kVp with a Rh target and 0.27 mm Cu filter. The SI in the detector was ~7000. This experiment was repeated 4 times. The error bars are a measure for the repeatability of the temporal instability. Based on our spectral model, the temporal response will result in an error in iodine uptake of ~8 % for a typical patient dose.

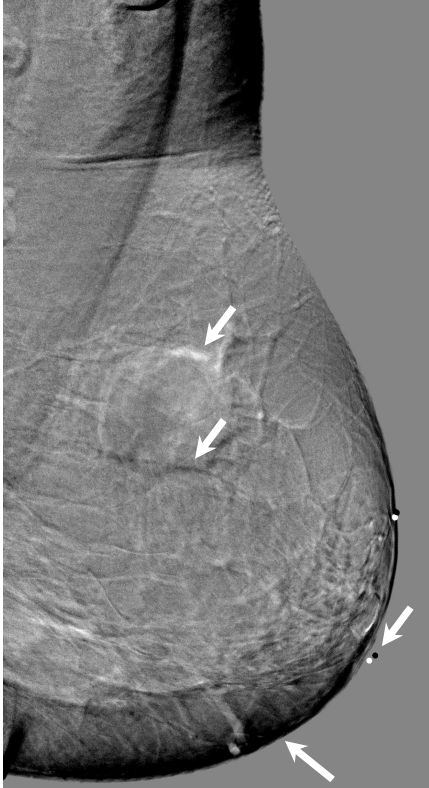


**Figure 9:** Example of patient movement. The image is the result of subtraction of a post-contrast projection image from a pre-contrast projection image. Two lead BBs were attached near the nipple. The arrows indicate patient motion.

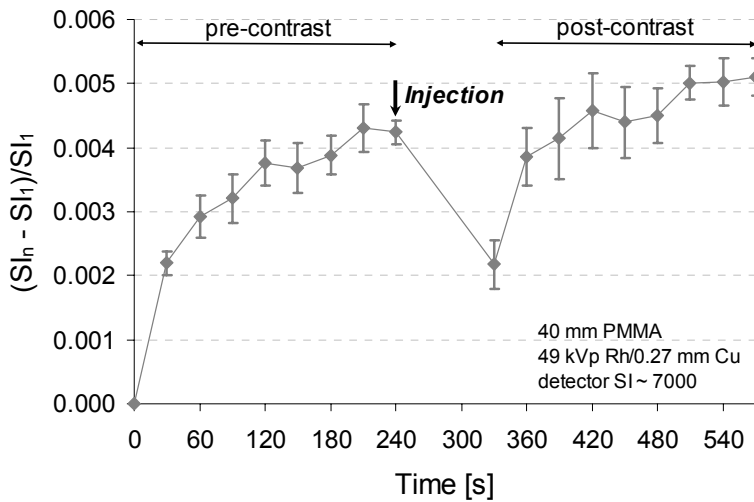


**Figure 10:** Example of the relative SI variation in a ROI of the nth image to the same ROI in the 1st image. The pre-contrast and post-contrast series each consist of an x-ray tube sweep in which 9 projection images are acquired. One image is acquired every 30 s. The first post-contrast image is acquired 90 s after the last pre-contrast image. The images were acquired under typical clinical conditions.

## 7. CONCLUSIONS

CE-DBT offers the potential to visualize the vascular characteristics of breast lesions as an adjunct to mammography. Based upon our initial clinical experience, and the work reported here, it is clear that the quantification of the iodine uptake for CE-DBT is complex. For the design of a CE-DBT system, attention should be paid to scatter and patient motion. At the current time, we are working on the reduction of patient motion and we are evaluating alternative subtraction methods using dual energy CE-DBT.

## ACKNOWLEDGEMENT

We would like to thank the financial support of Philips Medical Systems/RSNA Research Seed Grant 2005 and the National Cancer Institute Grant PO1-CA85484. We would like to thank General Electric Medical Systems for their technical help. Interested parties should contact the first author to obtain a copy of the spectral parameters.

## REFERENCES

1. Folkman, J., *The role of angiogenesis in tumor growth*. Seminars in Cancer Biology, 1992. **3**(2): p. 65-71.
2. Kaiser, W.A. and E. Zeitler, *MR imaging of the breast: fast imaging sequences with and without Gd-DTPA. Preliminary observations*. Radiology, 1993. **187**: p. 493-501.
3. Skarpathiotakis, M., et al., *Development of contrast digital mammography*. Medical Physics, 2002. **29**(10): p. 2419-26.
4. Jong, R.A., et al., *Contrast-enhanced digital mammography: Initial clinical experience*. Radiology, 2003. **228**: p. 842-850.
5. Lewin, J.M., et al., *Dual-energy contrast-enhanced digital subtraction mammography: Feasibility*. Radiology, 2003. **264**: p. 261-268.
6. Niklason, L.T., et al., *Digital tomosynthesis in breast imaging*. Radiology, 1997. **205**(2): p. 399-406.
7. Boone, J.M., T.R. Fewell, and R.J. Jennings, *Molybdenum, rhodium, and tungsten anode spectral models using interpolating polynomials with application to mammography*. Medical Physics, 1997. **24**(12): p. 1863-74.
8. [http://xdb.lbl.gov/Section1/Table\\_1-3.pdf](http://xdb.lbl.gov/Section1/Table_1-3.pdf).
9. Fahrig, R., et al., *Performance of glass fiber antiscatter devices at mammographic energies*. Medical Physics, 1994. **21**(8): p. 1277-82.
10. Jeunehomme, F., et al., *Controlling gray level variation in contrast enhanced digital mammography: design of a calibration procedure*. Proceedings of SPIE, Physics of Medical Imaging, 2003. **5030**: p. 338-348.